

*File Copy
R.A. #932950
R UN 235*

Copy 20
RM EL53F09a

FOR REFERENCE

NOT TO BE TAKEN FROM FILE

UNCLASSIFIED

NACA

RESEARCH MEMORANDUM

CLASSIFICATION CHANGED

for the

~~UNCLASSIFIED~~

U. S. Air Force

Authority of *NAAC 100* Date *11/19/58* *Notice No. 19*
DRAG AND STATIC STABILITY AT LOW LIFT OF ROCKET-POWERED
11/19/58
MODELS OF THE CONVAIR MX-1626 AIRPLANE AT
11/19/58
MACH NUMBERS FROM 0.7 TO 1.5

By James R. Hall and Russell N. Hopko

Langley Aeronautical Laboratory
Langley Field, Va.

~~CONFIDENTIAL~~ *11/7575*

Authority of *NAAC Records* Date *Jan 27, 1958*
Abstracts & Copies Notice No. 124
Effective Date, Jan 28, 1958
CLASSIFIED DOCUMENT *by JBC*

This material contains information affecting the National Defense of the United States within the meaning of the espionage laws, Title 18, U.S.C., Secs. 793 and 794, the transmission or revelation of which in any manner to unauthorized person is prohibited by law.

NATIONAL ADVISORY COMMITTEE

FOR AERONAUTICS

FILE COPY

WASHINGTON

To be returned to
the files of the Langley
Aeronautical Laboratory

JUN 11 1958

~~CONFIDENTIAL~~

UNCLASSIFIED



NATIONAL ADVISORY COMMITTEE FOR AERONAUTICS

RESEARCH MEMORANDUM

for the

U. S. Air Force

DRAG AND STATIC STABILITY AT LOW LIFT OF ROCKET-POWERED

MODELS OF THE CONVAIR MX-1626 AIRPLANE AT

MACH NUMBERS FROM 0.7 TO 1.5

By James R. Hall and Russell N. Hopko

SUMMARY

Flight tests have been made of 1/10-scale rocket-powered models of the proposed Consolidated Vultee Aircraft Corporation MX-1626 airplane with nacelles and without nacelles. Measurements were made of drag and static stability. These measurements revealed supersonic and transonic drag values at zero-lift conditions greater than anticipated. Measured and predicted values of $C_{m_{\alpha}}$ agree well. The presence of nacelles caused a decrease in $C_{m_{\alpha}}$ of about 0.002 at supersonic speeds and had no appreciable effect on the damping factor. All models were damped throughout the speed range of the tests. The trim angle was about -1° . A transonic trim change of about 1° occurred.

In order to explain the high drag measured in the foregoing tests, a 1/82.5-scale model having the same area distribution as the MX-1626 was tested, substantiating the results and giving credence to the area rule for airplane configurations. The subject airplane was "redesigned" to incorporate a cross-sectional area distribution which was designed to have less wave drag. The redesigned configuration had no large adverse interference effects.

A brief description of a ventral booster developed for the 1/10-scale model tests is included. Ventral boosters may be used to boost models to speeds which might be unattainable with conventional tandem boosters.

SECRET

UNCLASSIFIED

INTRODUCTION

A flight-test program of rocket-powered 1/10-scale models of the proposed Consolidated Vultee Aircraft Corporation MX-1626 supersonic bomber was carried out by the Pilotless Aircraft Research Division of the National Advisory Committee for Aeronautics at the request of the U. S. Air Force. The program concerned drag measurements and dynamic- and static-stability measurements. Herein are presented drag results of three models, a rough dummy model used in the booster development phase of the program, an instrumented configuration without nacelles, and an instrumented configuration with nacelles. Static-stability measurements are presented for the two instrumented configurations. The models were constructed by the Consolidated Vultee Aircraft Corporation and instrumented by the NACA. The tests were conducted at the Langley Pilotless Aircraft Research Station at Wallops Island, Va.

The drag measurements of the foregoing tests revealed drag levels which were considerably higher than anticipated at transonic and supersonic Mach numbers. In an effort to explain the phenomena, resort was made to the transonic area rule of reference 1, which states that the drag rise at transonic speeds is dependent upon the longitudinal area distribution. A 1/82.5-scale body of revolution with the same area progression as the subject airplane was tested to determine the applicability of the rule to fairly elaborate configurations. To further extend the application of the area-rule concept, an airplane configuration was designed by the NACA, after a later version of the MX-1626, to incorporate the principles of good area distribution. Results are presented of drag measurements of the foregoing models.

SYMBOLS

a_l	longitudinal acceleration, ft/sec ²
a_n	normal acceleration, ft/sec ²
a_t	lateral acceleration, ft/sec ²
a.c.	aerodynamic center, percent \bar{c}
b	span, ft
\bar{c}	mean aerodynamic chord, ft
C_D	coefficient of drag, Drag/ qS

C_{DB}	coefficient of base drag, $-\frac{P_B - P_S}{q} \frac{S_B}{S}$
C_{DL}	coefficient of drag due to lift, dC_D/dC_L^2
C_N	coefficient of normal force, taken equal to C_L at the low angles of attack used in these tests, Normal force/ qS
C_L	coefficient of lift, Lift/ qS
C_Y	coefficient of side force, Side force/ qS
C_m	coefficient of pitching moment about $\frac{1}{4} \bar{c}$, Pitching moment/ $qS\bar{c}$
C_n	coefficient of yawing moment, Yawing moment/ qSb
$(C_{m_q} + C_{m_{\dot{\alpha}}})$	damping factor, per radian, $\frac{dC_m}{d \frac{\dot{\theta} \bar{c}}{2V}} + \frac{dC_m}{d \frac{\dot{\alpha} \bar{c}}{2V}}$
I	moment of inertia, slug-ft ²
M	Mach number
P_S	static pressure, lb/ft ²
P_B	base pressure, lb/ft ²
P	period of the short-period oscillation, sec
q	dynamic pressure, lb/ft ²
R	Reynolds number
S	reference wing area, including area in fuselage, ft ²
S_B	base area of nacelle or pod, ft ²
$T_{1/2}$	time to damp to half amplitude, sec
V	velocity, ft/sec
W	model weight, lb
α	angle of attack, deg

β angle of yaw, deg

Subscripts:

X,Y,Z refer to longitudinal, lateral, and normal axes, respectively

α $d/d\alpha$, derivative with respect to α , per degree

β $d/d\beta$, derivative with respect to β , per degree

T refers to trimmed condition

APPARATUS AND TECHNIQUE

Models

A three-view drawing of the model configuration is given in figure 1. Details of the model components are given in figure 2 and tables I to III.

Model 1.- Model 1 was a noninstrumented nacelleless 1/10-scale dummy model used in the booster development phase preceding the actual tests. Model 1 was partially constructed of parts salvaged from a previous unsuccessful launching. Figure 3(a) shows the simplified contours used for expediency. The fuselage and pod were made integral and bolted to the wing, which was stripped of the original wood surface laminations, reducing the average thickness ratio at the mean-aerodynamic-chord station from 4 percent to 2.5 percent. The wing inboard leading edges behind the original antenna installation were ground to an approximate angle of 30° . The vertical tail section was welded to the wing and the triadic tail fins of hexagonal cross section with a thickness ratio of 0.05 were welded to the tail cone. The model was smoothly finished and coated with laquer.

Model 2.- Model 2 was an instrumented, nacelleless configuration, shown in figure 3(b). It was of composite magnesium-mahogany construction. The fuselage nose, tail sections, and pod tail section were of cast magnesium. The wing was constructed of mahogany bonded to a cast magnesium core. The fuselage center body and pod were of mahogany. The wooden surfaces of the model were finished smooth with Phenoplast and all surfaces were faired before the flight test.

Model 3.- Model 3, shown in figure 3(c), was instrumented and similar to model 2 except for the addition of mahogany nacelles, faired to a pointed nose, which were bolted to the wing.

Booster

An entirely new booster system was employed in the program due to the Mach number and instrumentation requirements. A three-view drawing of the booster is shown in figure 4. The size of the model was dictated by instrumentation considerations. A conventional tandem booster arrangement for such a model would not obtain the performance minimums required because of the weight and drag of the large booster fin area required for stability. Consequently, a ventral booster arrangement was utilized wherein the model fuselage nestled between two ABL Deacon rocket motors which were coupled at the rear. The thrust was imparted to the model through receptacles on the underside of the wing by projecting horns attached to the rocket motors. The receptacles beneath the model wing were equipped with spring-loaded covers which preserved the lower wing contour after booster-model separation.

Calculations, borne out by flight-test results, indicated a stable flight if the rocket nozzles were canted so that the thrust axis passed through the vertical position of the center of gravity of the model-booster combination at take-off. This produced zero pitching moment at take-off when the model had no aerodynamic stability, while with increasing Mach number the buildup of aerodynamic stability outpaced the destabilizing moment imparted by the upward movement of the center of gravity as rocket fuel was expended. In addition to canting the nozzles in the vertical plane, the nozzles were canted in the horizontal plane to pass through the center of gravity of the model-booster combination as a safeguard against excessive yaw induced by asymmetric thrust (particularly at rocket burnout).

A 15° rectangular flap of 20 square inches was provided at the midsection of each booster motor to increase the rate of translational separation of the booster from the model.

A nozzle-alining device was used to insure that the thrust axis passed through the center of gravity of the model-booster combination. The device is pictured schematically in figure 5. In use, the model-booster combination is fastened securely together and suspended from the hanger which is pinned at both ends. The combination center of gravity always positions itself below the axis of the hanger shaft, which is vertical. The nozzle arbors are inserted and alined with the hanger shaft at the base by manipulating the hanger adjusting screw. The arbors and hanger must lie in the same plane along their entire length if the nozzles are correctly canted in the vertical plane. Angularity between the arbors and the hanger is corrected by equally rotating each nozzle until the arbors and hanger are in the same plane. Deviation of the thrust axis from the longitudinal center of gravity is acceptable within limits in order to insure exact alinement with the vertical center of gravity.

A photograph of the model and booster on the launcher is shown in figure 6.

Instrumentation

Model 1 contained no internal instrumentation. Models 2 and 3 contained an NACA 10-channel telemeter which supplied continuous data throughout the flight. The internal instrumentation is given in table IV.

Data on velocity and decelerations were obtained with a CW Doppler velocimeter for all models. The flight path of the models was obtained by means of an SCR 584 radar set. Atmospheric conditions aloft were obtained by radiosonde. Wind velocity aloft was obtained by radar tracking of a reflector attached to the radiosonde balloon.

Pulse-Rocket Installation

Six small pulse rockets of approximately 6 lb-sec impulse were installed in the rear of the pod of models 2 and 3 to induce lateral disturbances throughout the flight which could be analyzed to obtain data on damping and stability. The pulse-rocket nozzles were flush with the contour of the model, exposing only three $\frac{1}{2}$ -inch holes on each side of the model, as seen in figure 3(c). The average thrust of the pulse rockets was 60 pounds and the burning time about 0.1 second, giving an effectively instantaneous disturbance in yaw to the model. The pulse-rocket nozzles were 1.96 feet behind the center of gravity of the model. Igniter delay squibs were provided to distribute the disturbances over the Mach number range of the flight test. Although the pulse rockets were installed primarily to cause a lateral disturbance, the rocket exhaust jet generated a pressure field on the lower wing surface, causing substantial pitching disturbances in addition to the lateral disturbances. The maximum amplitude of the oscillations was about the same in pitch and yaw, being from 1° to 5° and being greatest at transonic Mach numbers.

Technique

The models were boosted to supersonic speed and allowed to decelerate through the Mach number range from approximately 1.5 to 0.7. The coefficients of drag were obtained from CW Doppler velocimeter measurements in conjunction with radiosonde soundings of atmospheric conditions at the time of the test flight, as described in reference 2. The method of reference 2 was refined by the addition of a correction for the effect of winds aloft on the ground-referenced velocity of the model. The static

and dynamic pressures were also obtained from the ground radar measurements on model position and velocity. The longitudinal accelerometer data was used to obtain the coefficient of drag according to the expression

$$C_D = \frac{a_l}{g} \frac{W/S}{q}$$

A similar expression was used to evaluate normal and transverse force coefficients, using normal and transverse accelerations, respectively.

The base drag coefficient was determined for each nacelle and the pod base from the relationship

$$C_{DB} = - \frac{P_B - P_S}{q} \frac{S_B}{S}$$

The pressures were obtained by telemetry. The drag due to lift was calculated from telemetered values of C_N and wind-tunnel measurements of C_D/C_L^2 reported in reference 3.

The normal disturbances caused by the pulse rockets and by model-booster separation were analyzed to obtain the period and rate of decay of the oscillations. These data were then used to obtain the longitudinal static stability and damping factor, using the following expressions:

$$C_{m\alpha} = \frac{-I_Y}{57.3qSc} \left[\frac{4\pi^2}{P^2} + \left(\frac{0.693}{T_{1/2}} \right)^2 \right]_{\text{pitch}}$$

$$(C_{mq} + C_{m\dot{\alpha}}) = \frac{-4(0.693)I_Y V}{57.3qSc^2 T_{1/2}} + \frac{2I_Y C_{L\alpha}}{c^2} \frac{32.2}{W}$$

It was necessary to use wind-tunnel values for $C_{L\alpha}$ from reference 3 in the expression for damping factor in the absence of flight-test

measurements. The aerodynamic center was obtained from the expression $a.c. = \left(0.25 - \frac{C_{m\alpha}}{C_{L\alpha}}\right)$, again using wind-tunnel values of $C_{L\alpha}$. The values for $C_{n\beta}$ were calculated by using the single-degree-of-freedom expression from reference 4, namely

$$C_{n\beta} = \frac{I_Z}{57.3qSb} \left(\frac{4\pi^2}{p^2} \right)_{yaw}$$

This expression is shown in reference 5 to give good agreement with the values calculated by using the complete equations of motion.

ACCURACY

The accuracy estimated for the results presented is tabulated below:

Quantity	Accuracy at Mach number -		
	1.4	1.1	0.8
C_D	± 0.0005	± 0.0007	± 0.001
$C_{D\beta}$	± 0.0002	± 0.0003	± 0.0006
$C_{m\alpha}$	± 0.00025	± 0.00025	± 0.00025
$C_{n\beta}$	± 0.00020	± 0.00020	± 0.00020
$(C_{mq} + C_{m\dot{\alpha}})$	$\pm .4$	$\pm .4$	$\pm .4$
C_{N_T}	± 0.0019	± 0.0025	± 0.0055
C_{Y_T}	± 0.0001	± 0.00013	± 0.00028

RESULTS AND DISCUSSION

Drag

The Reynolds numbers of the tests are given in figure 7. The measured drag coefficient of model 1 (a rough nacelleless model) is given in figure 8. The measured drag of the dummy model was expected to give a good approximation of the drag of the refined model. Figures 9 and 10 present the results of the drag measurements made for models 2 and 3 (1/10-scale models of the MX-1626 without nacelles and with nacelles, respectively). The results indicate good agreement between models 1 and 2, substantiating the level of drag coefficient for the nacelleless configurations. A difference in C_D of about 0.0055 exists between the measured C_D and that predicted by the summation of the isolated drags of the components. One-tenth-scale transonic wind-tunnel tests by the NACA, not yet published, indicate that the difference may be attributed partly to high local interference drag due to landing-wheel fairings and partly to an unfavorable distribution of longitudinal area to be discussed in the appendix. Model 3 shows a difference in supersonic C_D of 0.0170 to 0.0130 between the level predicted by the summation of the isolated drags of the components and the measured zero-lift drag coefficient. An attempt to reduce this unusually high interference drag is presented in the appendix.

The base drag coefficients for models 2 and 3 are presented in figure 11.

Stability and Damping

Static stability.- Stability and damping are obtained from analysis of normal and transverse oscillations induced by the pulse rockets as explained in the section on "Technique." Typical oscillations as read from the telemetered records are shown in figure 12. It can be seen that no cross coupling exists between the lateral and longitudinal modes of motion of this oscillation. All other oscillations were also free of cross-coupling effects. The variation of C_{m_α} and C_{n_β} with Mach number for 1/10-scale models 2 and 3 is given in figure 13(a). Predicted values obtained from reference 6 and unpublished material from the Consolidated Vultee Aircraft Corporation are shown for comparison. Agreement of measured C_{m_α} with the predicted value is good. A sharp break in the C_{m_α} curve at Mach number 0.95 was measured for the complete configuration. It is not evident from these tests whether or not a similar sharp break exists for the nacelleless configuration. The magnitude of the decrease in static stability in pitch, due to the

addition of the nacelles, is substantiated qualitatively by reference 7. The addition of nacelles had no significant effect on $C_{n\beta}$ at supersonic speeds, but decreased $C_{n\beta}$ slightly below Mach number 1.0. Agreement with wind-tunnel tests (unpublished) is best at the higher speeds.

The static stability of models 2 and 3 is presented in terms of aerodynamic-center variation with Mach number in figure 13(b).

Damping.- The time required for the short-period oscillations induced by the pulse rockets to damp to half amplitude is given for models 2 and 3 in figure 14(a). Both models were always damped in pitch and yaw. The effect of the nacelles is seen to be quite small in pitch. In yaw, the time to damp the nacelleless configuration experiences a sharp oscillation through the transonic range. The damping-in-pitch factor ($C_{m\dot{q}} + C_{m\dot{\alpha}}$) per radian, is given in figure 14(b). The difference between the two curves is within the experimental accuracy of the measurement. Agreement between the two models is quite good for this type of measurement. Reference 8 shows the smoother curve of model 2 to be more typical of the delta wing than the reflexed curve of model 3.

Trim, lift, and yaw coefficients.- The variation of C_{N_T} and C_{Y_T} with Mach number for models 2 and 3 are presented in figure 15. The variation of trim side force with Mach number is smooth and the difference between the values for the two models is believed to be due to the manufacturing tolerances. Model 2 exhibits a smooth variation of C_{N_T} throughout the Mach number range. The effect of the nacelles is to cause a decrease of trim lift coefficient. The decrease corresponds to about 1° angle of attack at supersonic speeds. The trim angle increases through the transonic range and decreases again at subsonic speeds. A trim change occurs through the transonic range corresponding to about 1° . The negative angle of incidence of the large nacelles is probably a major cause of the difference in the level of trim lift coefficients between the two models.

CONCLUSIONS

1. The drag level of the MX-1626 airplane was considerably higher than the value predicted neglecting interference drag.

2. A "redesign" of the subject configuration, utilizing a more gradual progression of cross-sectional area in conjunction with clean aerodynamic components, greatly reduced adverse interference effects.

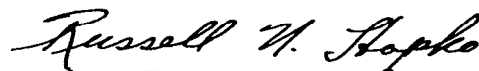
3. Measured and predicted values of C_{m_α} agree well. The presence of nacelles caused a decrease in C_{m_α} of about 0.020 throughout the supersonic range. The presence of nacelles had no significant effect on $C_{n\beta}$.
4. The MX-1626 model was damped throughout the speed range of the tests. The presence of nacelles had no appreciable effect on the damping factor.
5. The MX-1626 trimmed at about -1° angle of attack and experienced a trim change through the transonic range of about 1° .
6. Ventral boosters may be used to boost models to speeds which might be unattainable with conventional tandem boosters.

Langley Aeronautical Laboratory,
National Advisory Committee for Aeronautics,
Langley Field, Va., May 25, 1953.



James R. Hall

Aeronautical Research Scientist



Russell N. Hopko

Aeronautical Research Scientist

Approved:



Joseph A. Shortal

Chief of Pilotless Aircraft Research Division

cg

APPENDIX

APPLICATION OF THE TRANSONIC AREA RULE TO REDUCE THE
INTERFERENCE DRAG OF AN AIRPLANE CONFIGURATION

In an effort to explain the unusually high interference drag experienced in the foregoing tests, resort was made to the area rule of reference 1. The rule states that the drag rise of a configuration is primarily dependent upon its longitudinal area development. In order to test the applicability of the rule to the relatively complicated shape of the subject configuration, a 1/82.5-scale body of revolution with the same axial area distribution was tested. Hereinafter, this model will be called model 4. The area distribution of the MX-1626 is shown in figure 16. Figure 17 shows a low-drag area distribution to be discussed later. A phantom view of model 4 is shown in figure 18. The volumes of the stabilizing fins are included in the area development. The model was flown from a 6-inch helium gun at Wallops Island and the drag obtained by radar. The results of the drag measurements on this model are shown in figure 19, compared with the zero-lift drag measurements of model 3. The extremely good agreement lent credence to the applicability of the method for predicting the transonic drag rise of complete airplane configurations.

Since the high supersonic drag characteristics of the subject configuration could be apparently assigned to its unfavorable area distribution, a logical extension of the program was to redesign the subject configuration to improve the area distribution. This was done on the basis of the then latest version of the MX-1626, called the MX-1964, which incorporated the following modifications over the subject version:

	MX-1626	MX-1964
Wing	1,200 ft ² , 65° delta, 4-percent thickness ratio	1,400 ft ² , 60° delta, 4.5-percent thickness ratio
Nacelles	Two large nacelles located on top of wing	Four nacelles in siamese pairs, underslung
Tails	<ul style="list-style-type: none"> Vertical delta tail on fuselage Triadic swept tails on pod 	<ul style="list-style-type: none"> Vertical swept tail on fuselage Single vertical tail on pod. Small delta wing forward under main wing. Canard pitch control
Fuselage	900 inches long	1,051 inches long

The area distribution of the MX-1964 is shown as the dashed line in figure 16. Note that its area distribution is at least equally as conducive to high wave drag as that of the MX-1626.

In the "redesign" effort, supersonic aerodynamic factors and internal volume requirements were given primary consideration over structural and balance problems. It was appreciated that the design of a workable airplane is a vastly complicated endeavor and the simplified approach used herein aimed at nothing more than the validation of the area rule for a complete airplane configuration. If the concept could be shown to be effective, it was felt that its practical application was a problem for industrial design teams.

Aiming at a transonic drag rise of about 0.01, the redesign was accomplished, using as a basis a low-drag parabolic body of revolution (ref. 9) of fineness ratio 9, with the maximum diameter located at 50 percent of the length. The optimum ratio of base diameter to maximum diameter was fixed at 0.2 from the work of W. E. Stoney, Jr., as yet unpublished. Relocation of the components of the MX-1964 in order to fulfill the desired area progression is shown in figure 17 and includes the following:

- (1) Separating and staggering the nacelles to avoid their sudden concentration of area.
- (2) Relocation of the tails.
- (3) Relocation of the wing and reduction of thickness ratio to 3 percent. A diamond plan form was used instead of a delta plan form because of the slightly less abrupt rate of area decrease at the rear of the wing. The area was increased from 1,400 square feet to 1,543 square feet by sweeping the trailing edge 10° from the tip.
- (4) Increase in maximum diameter and volume of the body.
- (5) Avoidance of external landing-wheel fairings.

The redesigned aircraft is larger than its predecessor in volume by 60 percent and in wing area by 28 percent but it fulfills the requirement of good area distribution. By scaling down the size to attain a wing area comparable to the MX-1626, the two airplanes could be directly compared on the basis of drag coefficient.

With this comparison in mind, the area distribution of figure 17 was applied to a simplified airplane configuration and a 1/15-scale model constructed. The model, hereinafter called model 5, is shown in the three-view drawing of figure 20. The photographs of figure 21 show this model in top view and side view. The model was flight-tested to

a Mach number of 1.35 and drag measurements were made with CW Doppler velocimeter equipment. Figure 22 shows the model on the launcher prior to launching.

As a further check on the area-rule concept a sixth model, hereinafter called model 6, was tested, being a 1/82.5-scale body of revolution with the same longitudinal area distribution as the redesigned airplane configuration (model 5). A photograph of the model is shown in figure 23. The model was flown from the 6-inch helium gun and the drag obtained by radar.

External drag-coefficient measurements of model 5 are compared in figure 24 with the external drag coefficient predicted by the summation of the isolated component drags. Also shown is the drag-coefficient measured for model 6 corrected to the skin friction of model 5. The good agreement between models 5 and 6 again substantiates the fact that it is possible to duplicate the wave drag of an airplane by a comparatively simple body of revolution having the same area distribution. Comparing models 5 and 3, it is seen that a 1/2 to 1/3 reduction of drag coefficient is effected by the application of the area-rule concept. Although the drag measurements of model 5 show a virtual elimination of interference drag, additional savings may be possible in the form of favorable interference effects. It is interesting to note that the measured drag level of models 4, 5, and 6 persists well into the supersonic range, indicating the validity of area-rule concepts beyond the transonic range.

REFERENCES

1. Whitcomb, Richard T.: A Study of the Zero-Lift Drag-Rise Characteristics of Wing-Body Combinations Near the Speed of Sound. NACA RM L52H08, 1952.
2. Morrow, John D., and Katz, Ellis: Flight Investigation at Mach Numbers From 0.6 to 1.7 To Determine Drag and Base Pressures on a Blunt-Trailing-Edge Airfoil and Drag of Diamond and Circular-Arc Airfoils at Zero Lift. NACA RM L50E19a, 1950.
3. Lavender, R. E., Bauman, W. A., and Griffith, B. J.: Project MX-1626 - An Analysis of Wind Tunnel Lift and Drag Data. Rep. No. FZA-4-038 (Contract AF 33(038)-21250), Consolidated Vultee Aircraft Corp., Sept. 11, 1952.
4. Bishop, Robert C., and Lomax, Harvard: A Simplified Method for Determining From Flight Data The Rate of Change of Yawing-Moment Coefficient With Sideslip. NACA TN 1076, 1946.
5. Purser, Paul E., and Mitchell, Jesse L.: Miscellaneous Directional-Stability Data for Several Airplane-Like Configurations From Rocket-Model Tests at Transonic Speeds. NACA RM L52E06b, 1952.
6. Stability and Control Group: Preliminary Stability and Control Analysis of the Supersonic Bomber-Reconnaissance Airplane. Rep. No. FZA-043, Consolidated Vultee Aircraft Corp., Jan. 25, 1951.
7. Jacobsen, Carl R.: Effects of the Spanwise, Chordwise, and Vertical Location of an External Store on the Aerodynamic Characteristics of a 60° Delta Wing at Mach Numbers of 1.41, 1.62, and 1.96. NACA RM L52H29, 1952.
8. Gillis, Clarence L., and Chapman, Rowe, Jr.: Summary of Pitch-Damping Derivatives of Complete Airplane and Missile Configurations As Measured in Flight at Transonic and Supersonic Speeds. NACA RM L52K20, 1953.
9. Hart, Roger G., and Katz, Ellis R.: Flight Investigations at High-Subsonic, Transonic, and Supersonic Speeds To Determine Zero-Lift Drag of Fin-Stabilized Bodies of Revolution Having Fineness Ratios of 12.5, 8.91, and 6.04 and Varying Positions of Maximum Diameter. NACA RM L9I30, 1949.

TABLE I.- FUSELAGE GEOMETRY

[Refer to figure 2 for symbol key]

Fuselage station	A	B	C	Fuselage sections at respective fuselage stations					
				Height	Ordinate	Height	Ordinate	Height	Ordinate
5.000 10.000	1.600 2.750	1.350 2.565							
13.775	3.470	3.480		0 .100 .200 .400 .600	1.294 1.489 1.579 1.669 1.720	0.830 1.300 1.800 2.300 2.800	1.735 1.700 1.609 1.444 1.160	3.100 3.250 3.400 3.480	0.870 .675 .380 0 R = 0.912
14.780 16.000 17.000 18.000 19.000	3.630 3.830 3.980 4.140 4.268	3.940 4.510 4.975 5.430 5.670							
20.000	4.440	5.750		0 .050 .100 .400 .840	1.920 2.030 2.075 2.190 2.220	1.400 2.100 2.800 3.470	2.190 2.080 1.875 1.615	4.135 4.591 5.000 5.750	1.340 1.150 .950 0 R = 0.912
22.500 25.000 30.492	4.800 5.180 5.760	5.750 5.750 5.750							
35.000 to 50.000	5.980	5.750		0 .400 .800 1.500	2.990 2.970 2.930 2.785	2.200 2.900 3.600	2.570 2.290 1.940	4.300 5.000 5.750	1.530 1.040 0 R = 0.912
56.000	5.640	5.545	0.277						
60.000	5.140	5.240	0.441	.441 .800 1.200 1.900	2.570 2.540 2.480 2.310	2.570 3.300 4.000	2.050 1.725 1.330	4.600 5.240	.900 0 R = 0.700
65.000	4.200	4.744	2.100						
70.000	2.980	4.190	1.490	.924 1.200 1.600	1.490 1.480 1.420	2.200 2.800 3.400	1.274 1.030 .720	3.900 4.190	.380 0 R = 0.287
75.000 77.500 79.000 80.000	1.620 .760 .314 0	3.600 3.300 3.120 3.012	1.245 1.658 2.235 2.700						

TABLE II.- NACELLE GEOMETRY

[Refer to figure 2 for symbol key]

Nacelle station	Radius A	Radius B	C
-6.000	0	-----	0
-2.440	.940	-----	1.908
-.621	1.420	-----	2.840
0	1.545	-----	3.090
.950	1.730	-----	3.460
2.000	1.895	0.490	3.885
5.000	2.265	1.120	4.890
8.000	2.485	1.580	5.580
11.000	2.590	1.900	6.000
13.300	2.600	2.050	6.165
16.000	2.600	2.125	6.230
19.000	2.600	2.103	6.200
22.000	2.600	2.000	6.100
25.000	2.580	1.849	5.913
28.000	2.520	1.655	5.640
31.000	2.430	1.410	5.273
34.000	2.265	1.130	4.815
37.000	2.055	2.840	4.270
40.000	1.780	.530	3.628
42.000	1.562	-----	3.125



TABLE III.- POD GEOMETRY

[Refer to figure 2 for symbol key]

Pod station	A	B	Radius C	L	Radius R	S
0	1.225	-----	-----	-----	0	-----
8.200	2.700	0	-----	-----	1.240	-----
20.000	4.450	1.122	-----	-----	2.210	-----
30.000	5.540	2.088	-----	-----	2.830	-----
40.000	5.990	2.910	-----	-----	3.000	-----
50.000	6.000	3.000	-----	6.000	3.000	0
58.000	5.850	3.000	1.635	5.967	3.000	.087
70.000	5.208	3.000	2.000	5.736	3.000	.521
80.000	4.494	-----	2.208	4.578	2.676	1.046
90.000	2.568	-----	-----	2.568	1.434	-----



TABLE IV.- INTERNAL INSTRUMENTATION OF MODELS

Instrument	Purpose	Location	Range
Total pressure } Static pressure }	Mach number, altitude, and Reynolds number	Sting	80 to 20 psi abs
			15 to 5 psi abs
Left nacelle base pressure } Right nacelle base pressure }	Nacelle base drag on model 3 only	1/2 radius above center on vertical center line	15 to 5 psi abs
		1/2 radius below center on vertical center line	15 to 5 psi abs
Pod base pressure	Base drag	Center 1.2 in. inside base. Base sealed by bulkhead 1.3 in. from base	15 to 5 psi abs
Longitudinal accelerometer; low sensitivity } Longitudinal accelerometer; high sensitivity }	C_D	Inside pod at c.g.	+1 g to -6g
			+1 g to -3g
Normal accelerometer	C_N	Inside pod at c.g.	+10g to -10g
Normal accelerometer	C_N and tail buffet	At pod tail 1.96 ft from c.g.	+10g to -10g
Transverse accelerometer	C_y	Inside pod at c.g.	+5g to -5g
Transverse accelerometer	C_y (replaces one nacelle base- pressure channel in model 3)	At pod tail 1.98 ft from c.g.	+5g to -5g

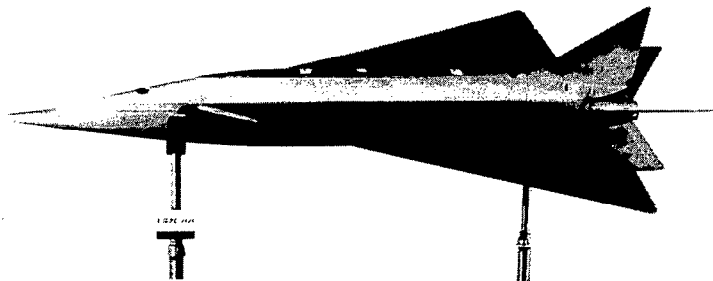


TABLE V.- PHYSICAL CHARACTERISTICS OF AIRPLANE CONFIGURATION MODELS

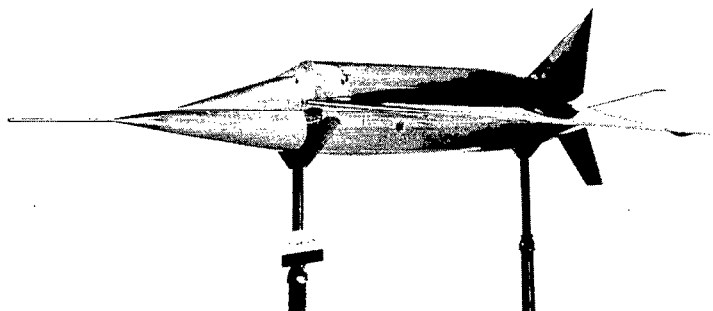
Model number	1	2 (a)	3 (a)	5
Scale	1/10	1/10	1/10	1/15
\bar{c} , ft	3.38	3.38	3.38	2.40
S, ft ²	12	12	12	6.85
Weight, lb	224	234.5	241	105.7
I _x , slug-ft ²	^b 3.5	3.9	2.3	-----
I _y , slug-ft ²	^b 22	24.4	23.4	-----
I _z , slug-ft ²	^b 19	20.68	20.1	-----
Long c.g. location, percent of M.A.C.	0.25	0.25	0.25	0.06
Vertical c.g. location, measured from parting plane, in.	-----	-0.012	+0.50	On x-axis
Faired nacelle base area, ft ²	0.0578	0.0578	0.0578	-----
Pod base area, ft ²	0.0449	0.0449	0.0449	-----

^aModels 2 and 3 were telemetered.
^bEstimated.

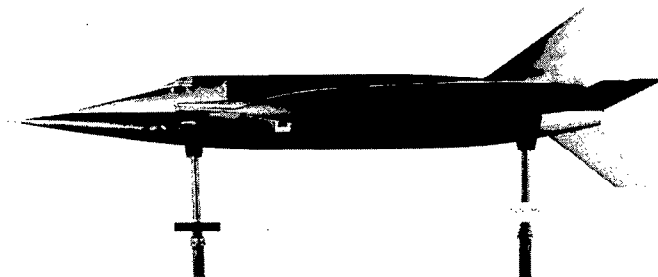




(a) Model 1.  L-76423



(b) Model 2.  L-77590



(c) Model 3.  L-76761

Figure 3.- Photographs of 1/10-scale models and dummy model of proposed Consolidated Vultee Aircraft Corporation MX-1626 airplane.

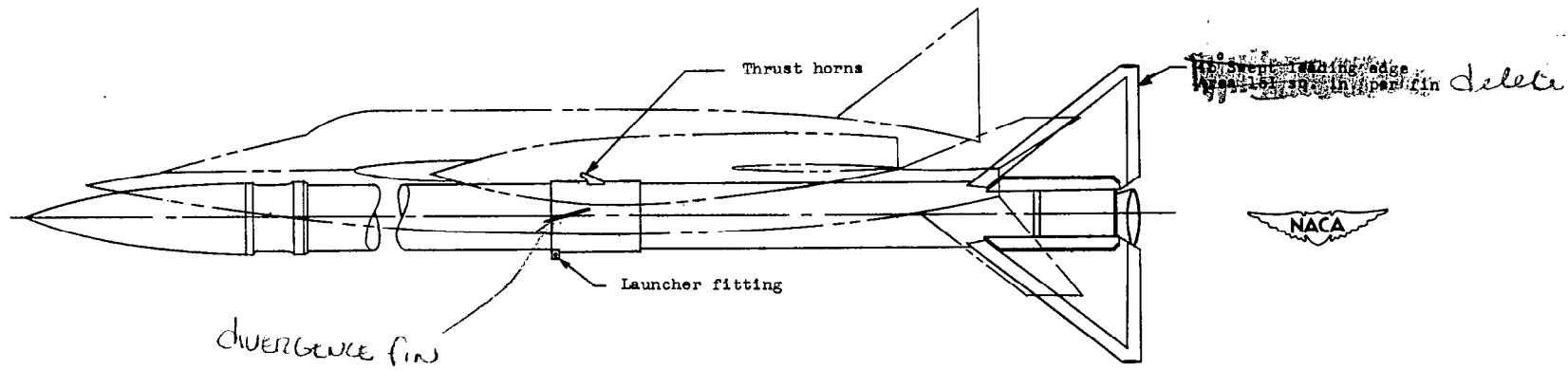
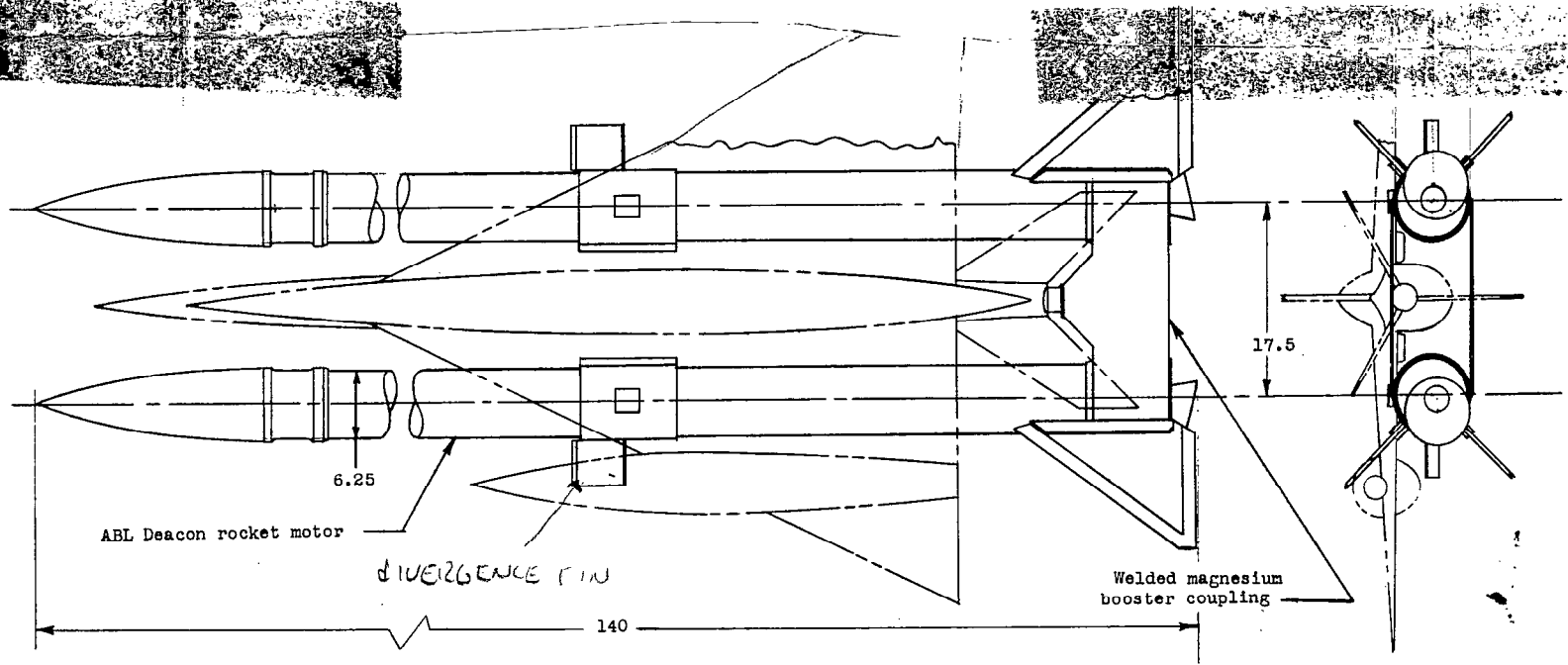


Figure 4.- Three-view drawing of ventral booster used in the subject tests. Dimensions in inches.

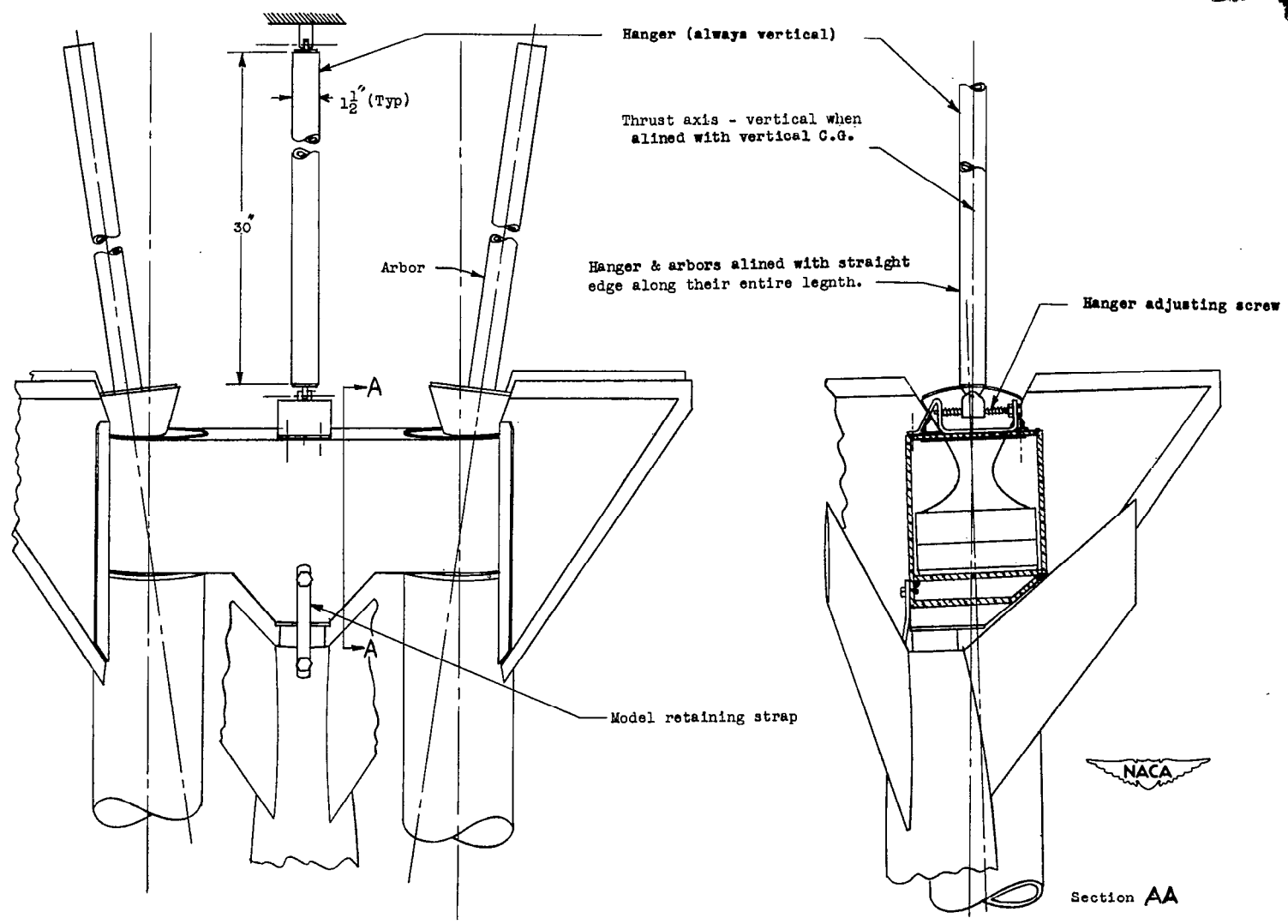


Figure 5.- Sketch of nozzle-alining device used to aline thrust axis with vertical center of gravity.

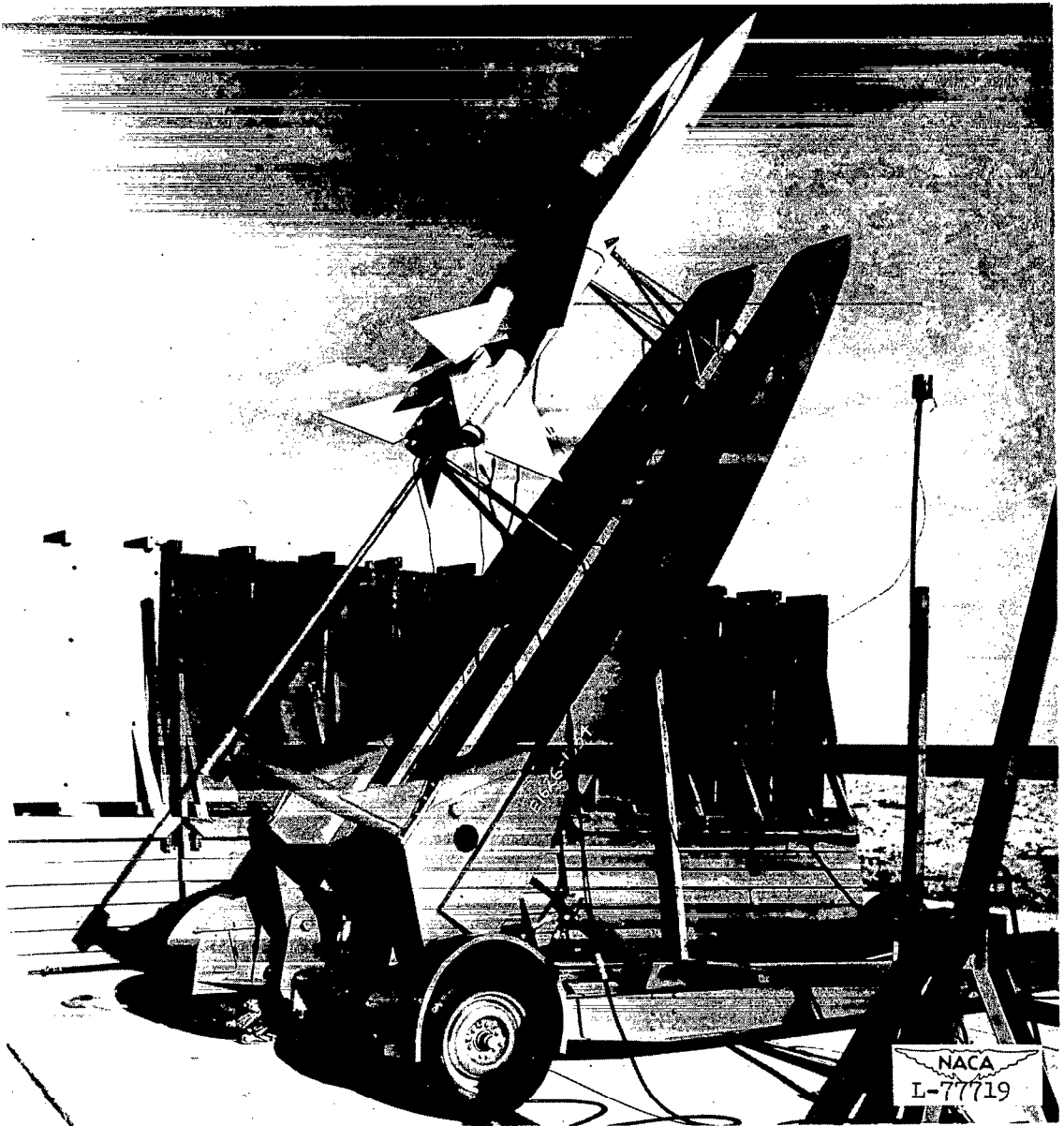


Figure 6.- Model 2 and booster on launcher. Arrangement typical of all 1/10-scale models.

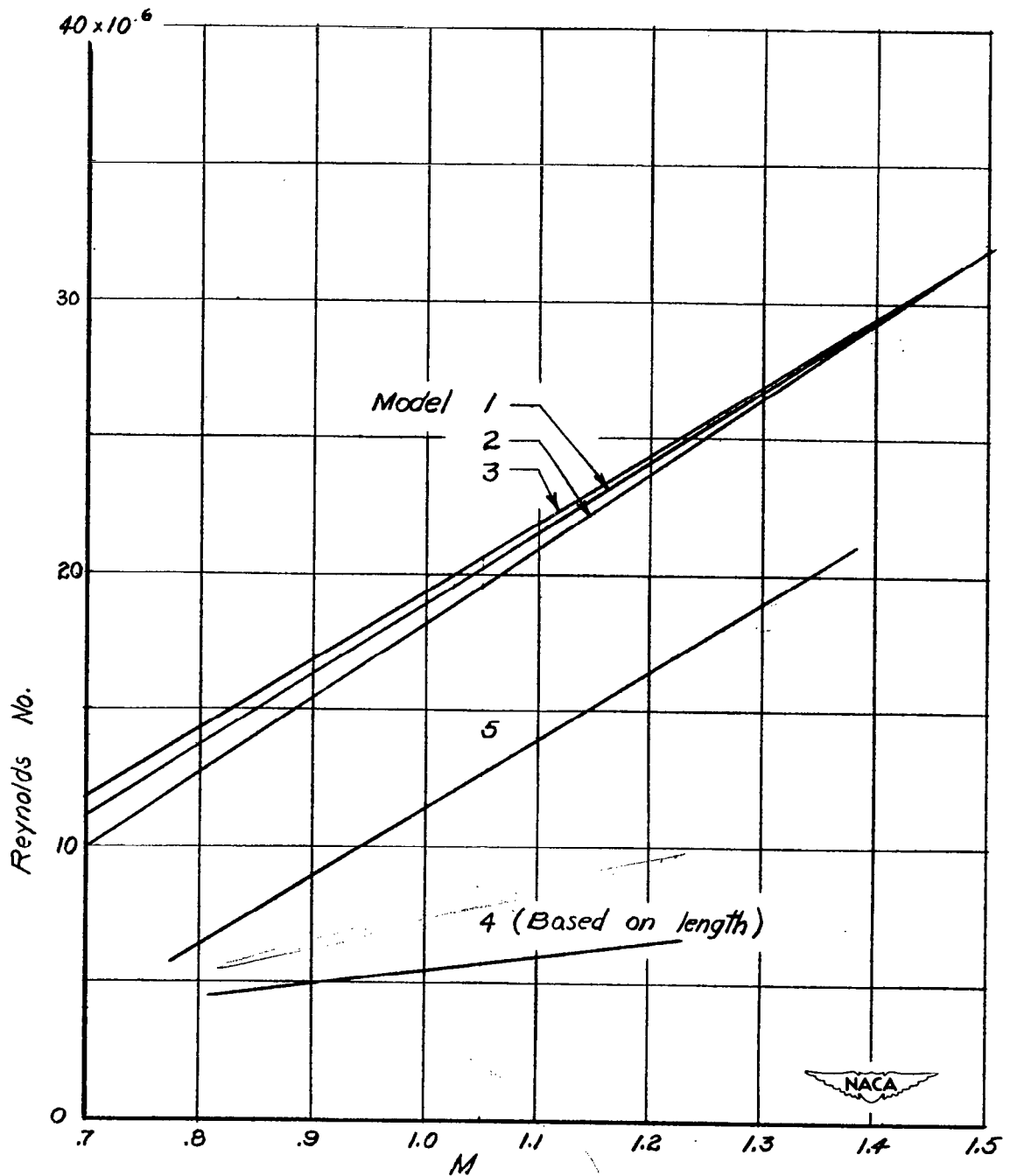


Figure 7.- Reynolds number range of flight tests. Based on \bar{c} except where noted.

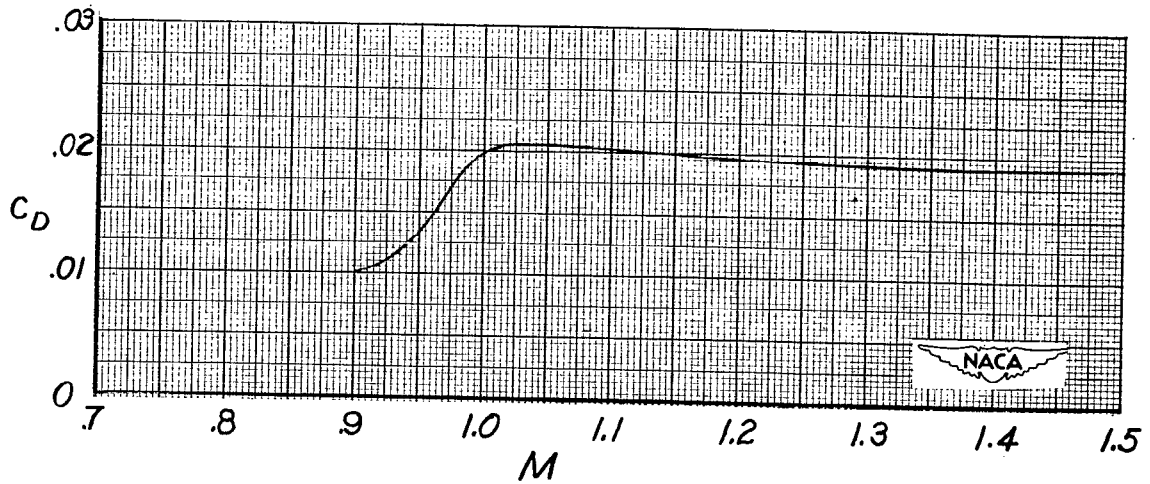


Figure 8.- Drag coefficient measured for model 1.

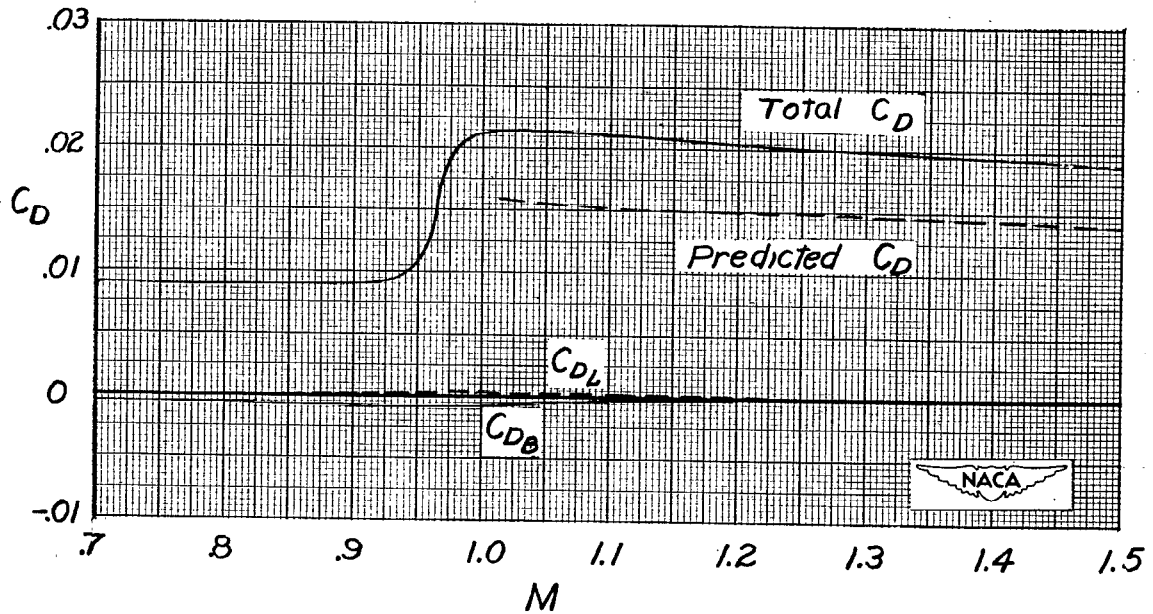


Figure 9.- Measured drag coefficients and predicted drag coefficient for model 2. Predicted drag coefficient does not include base pressure.

x no base drag, closed nacelles, no pod drag
16'

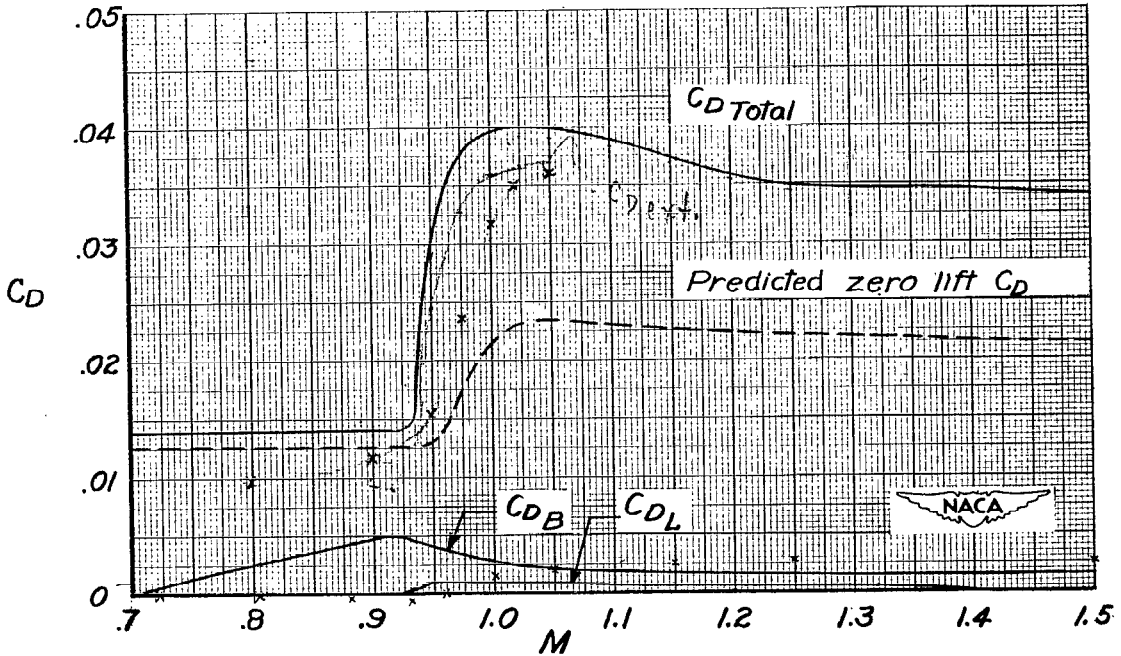
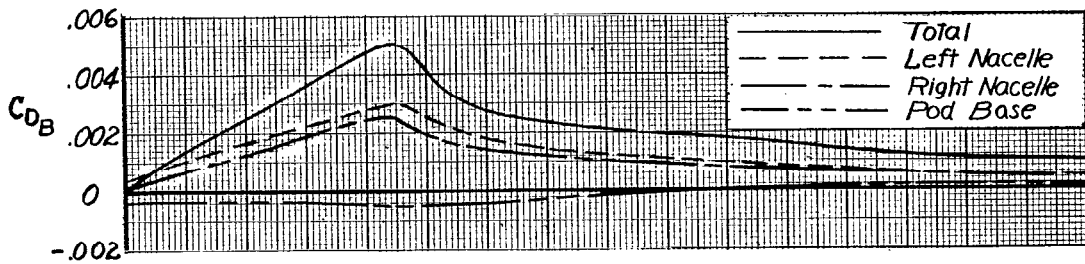
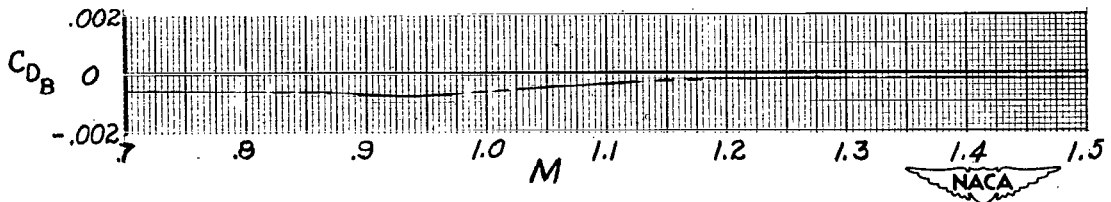


Figure 10.- Drag coefficient measured for model 3.



(a) Model 3.



(b) Model 2.

Figure 11.- Base pressure coefficients measured in tests. Left-nacelle pressure tap was located 1/2 radius above center of base. Right-pod base-pressure tap was located at center of pod base.

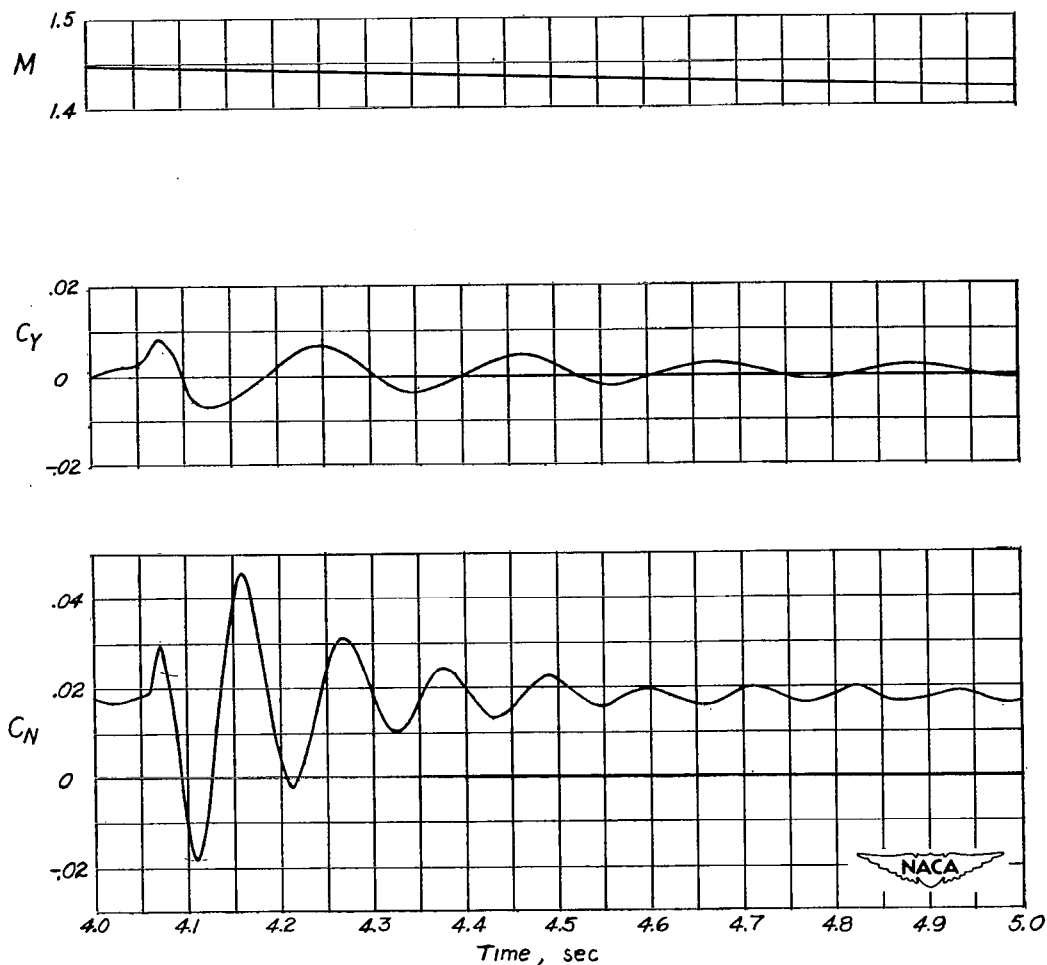
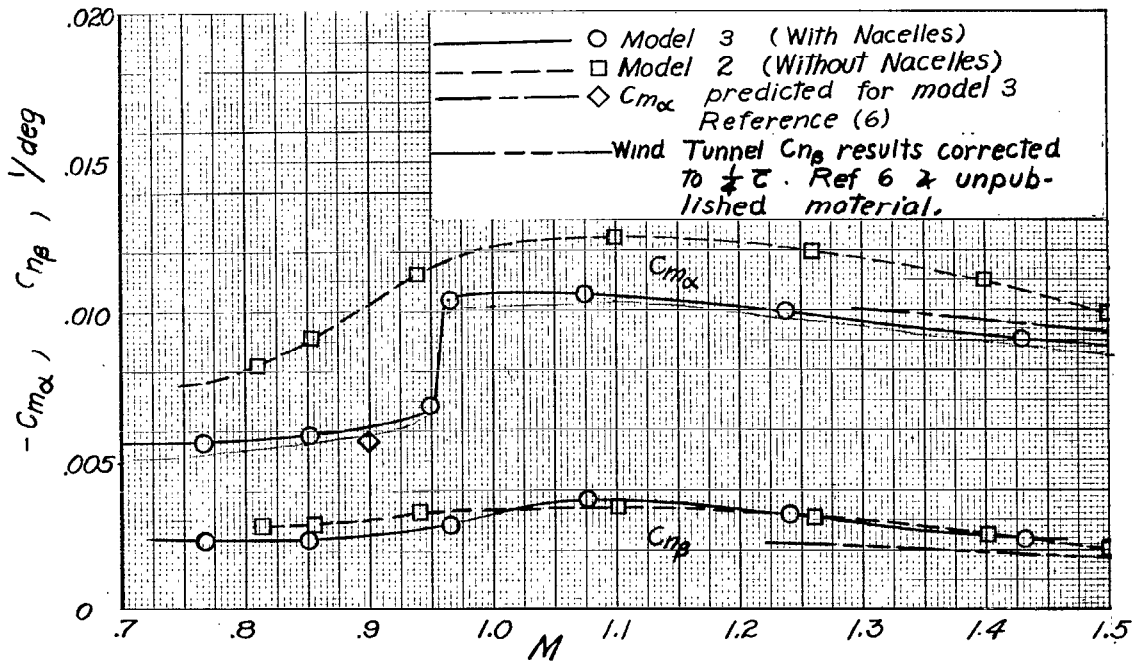
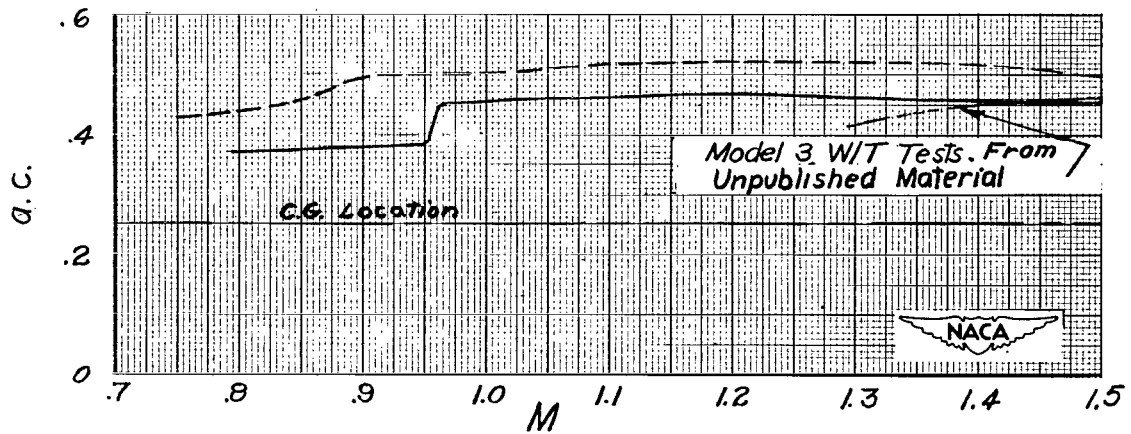


Figure 12.- Variation of force coefficients and Mach number taken from a portion of a typical oscillation. Note the absence of any cross coupling between the two modes of motion.

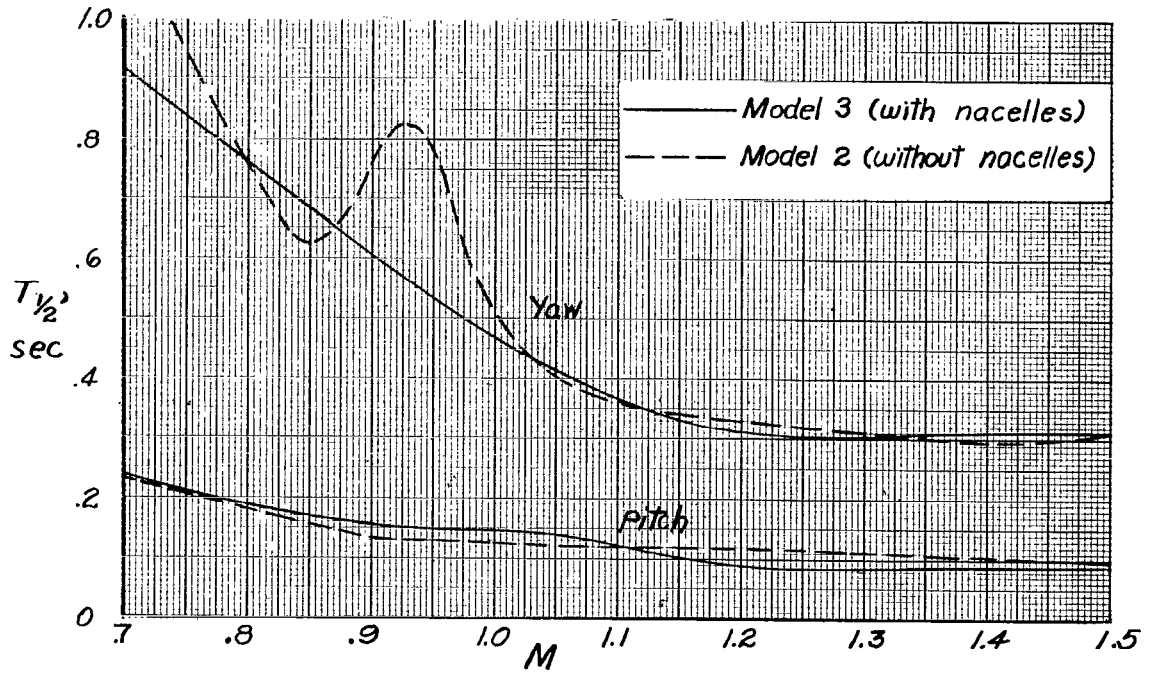


(a) Variation of static stability with Mach number.

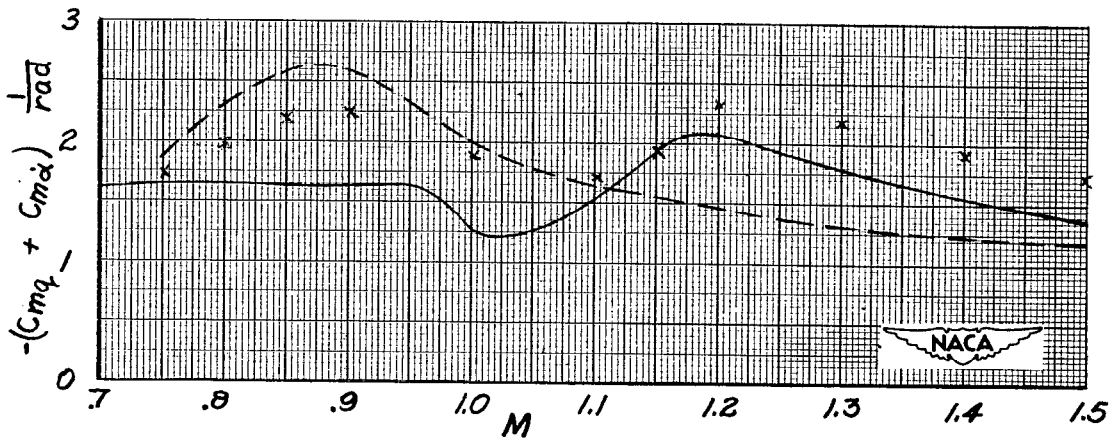


(b) Variation of aerodynamic center with Mach number.

Figure 13.- Variation of static stability characteristics with Mach number.

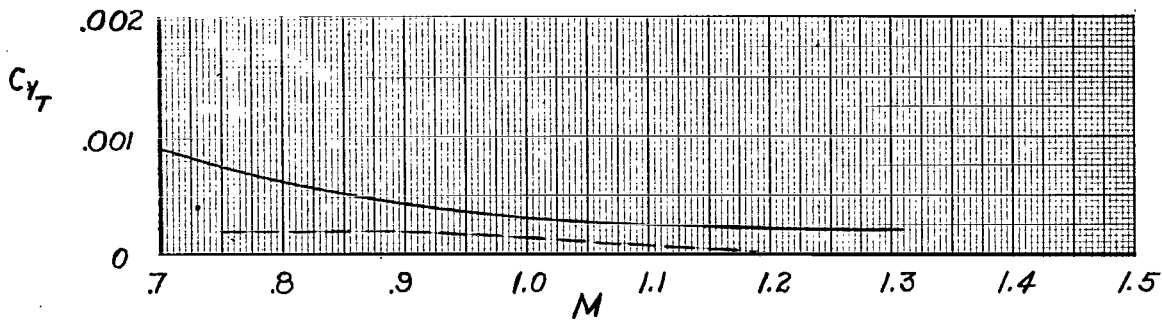


(a) Variation of time to damp to half amplitude with Mach number.

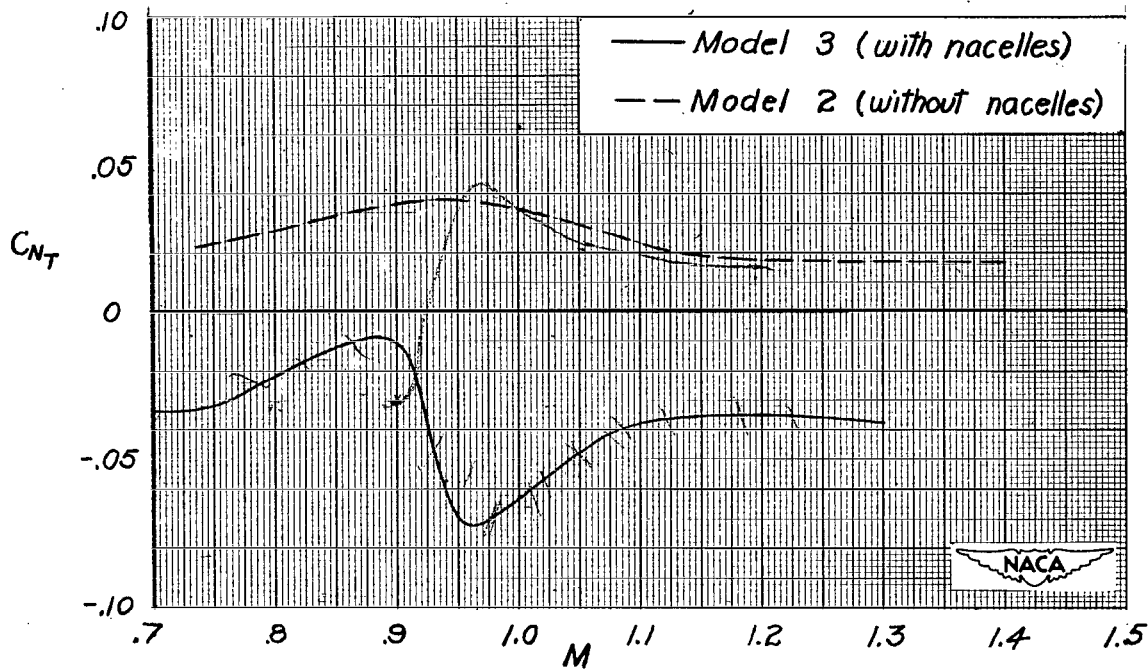


(b) Variation of pitch damping factor with Mach number.

Figure 14.- Variation of damping characteristics with Mach number for models 2 and 3.



(a) Trim yaw coefficients.



(b) Trim lift coefficients.

Figure 15.- Variation of trim lift and yaw coefficients with Mach number for models with and without nacelles.

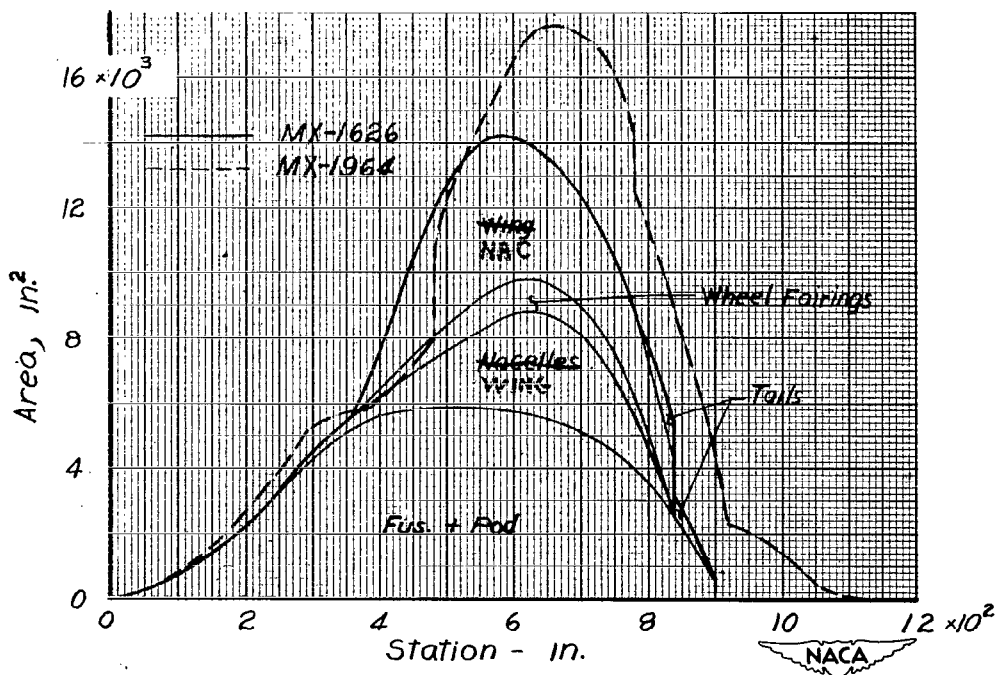


Figure 16.- Area distribution of MX-1626. Note the high slopes of forebody and afterbody in each case.

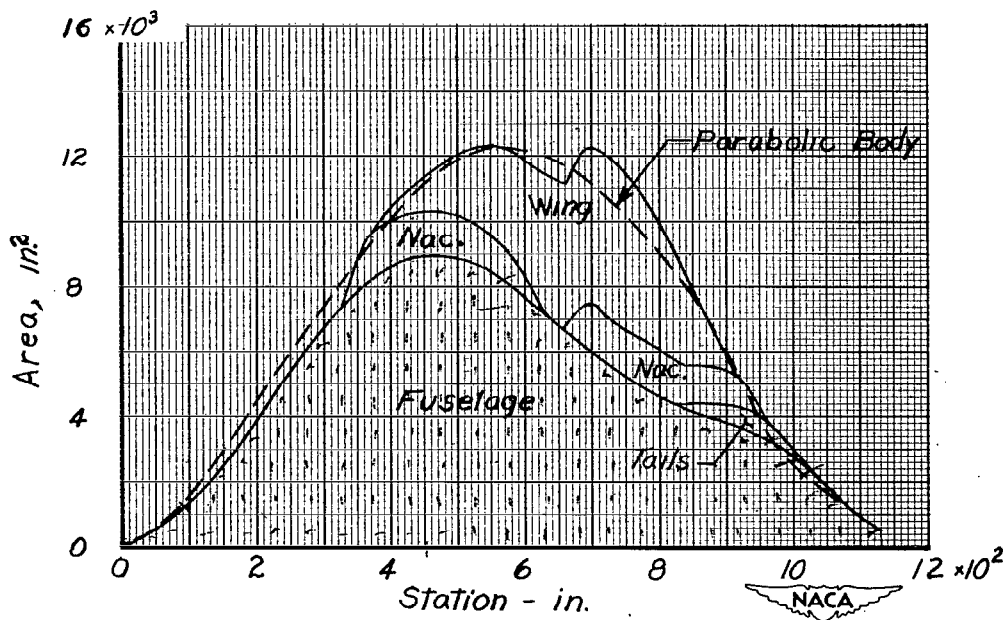


Figure 17.- Full-scale area distribution of model 5 showing proximity to low-drag parabolic body of revolution.

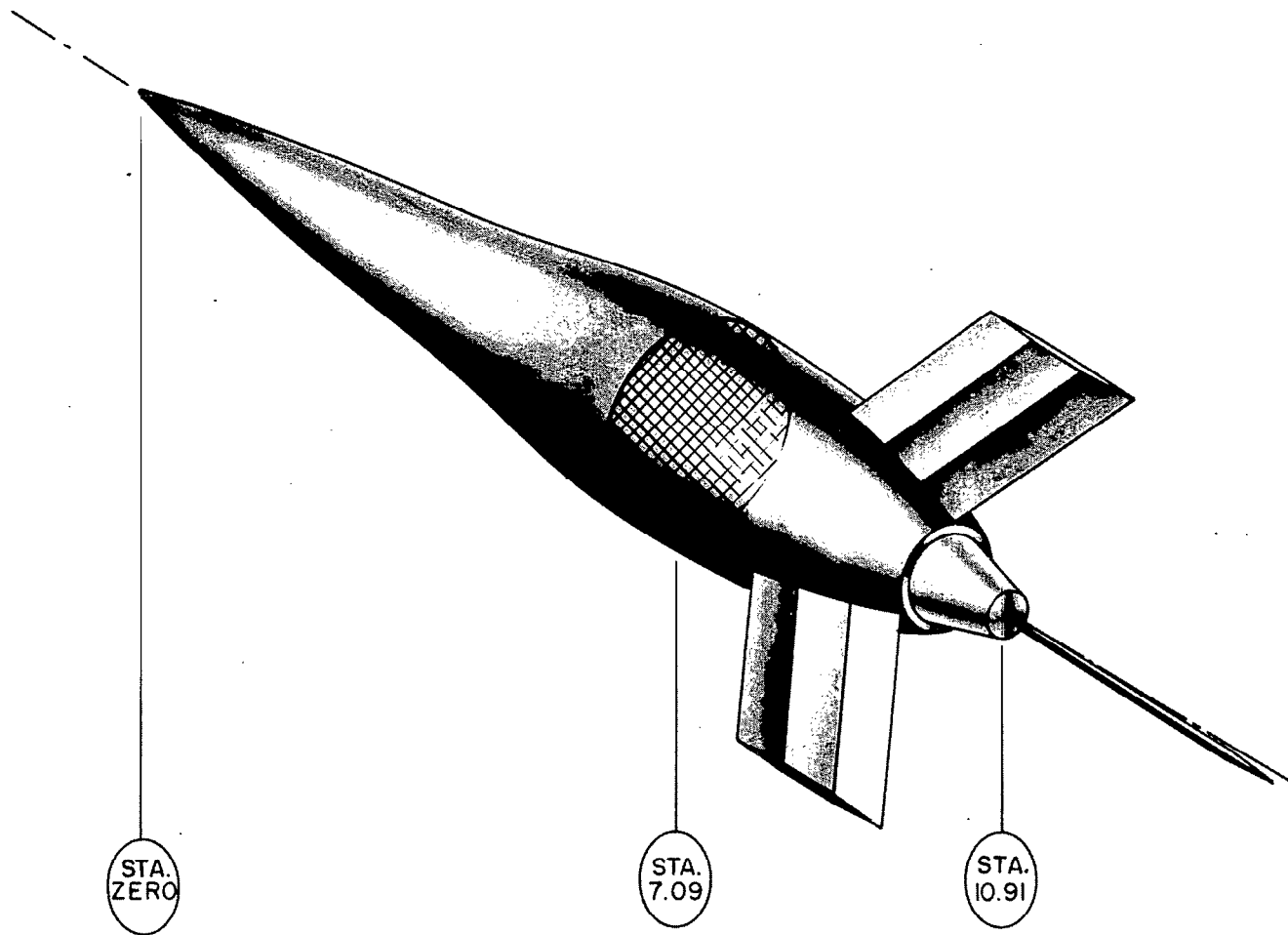


Figure 18.- Phantom view of test model 4. Model is 1/82.5-scale body of revolution with area distribution of the MX-1626.



L-80205

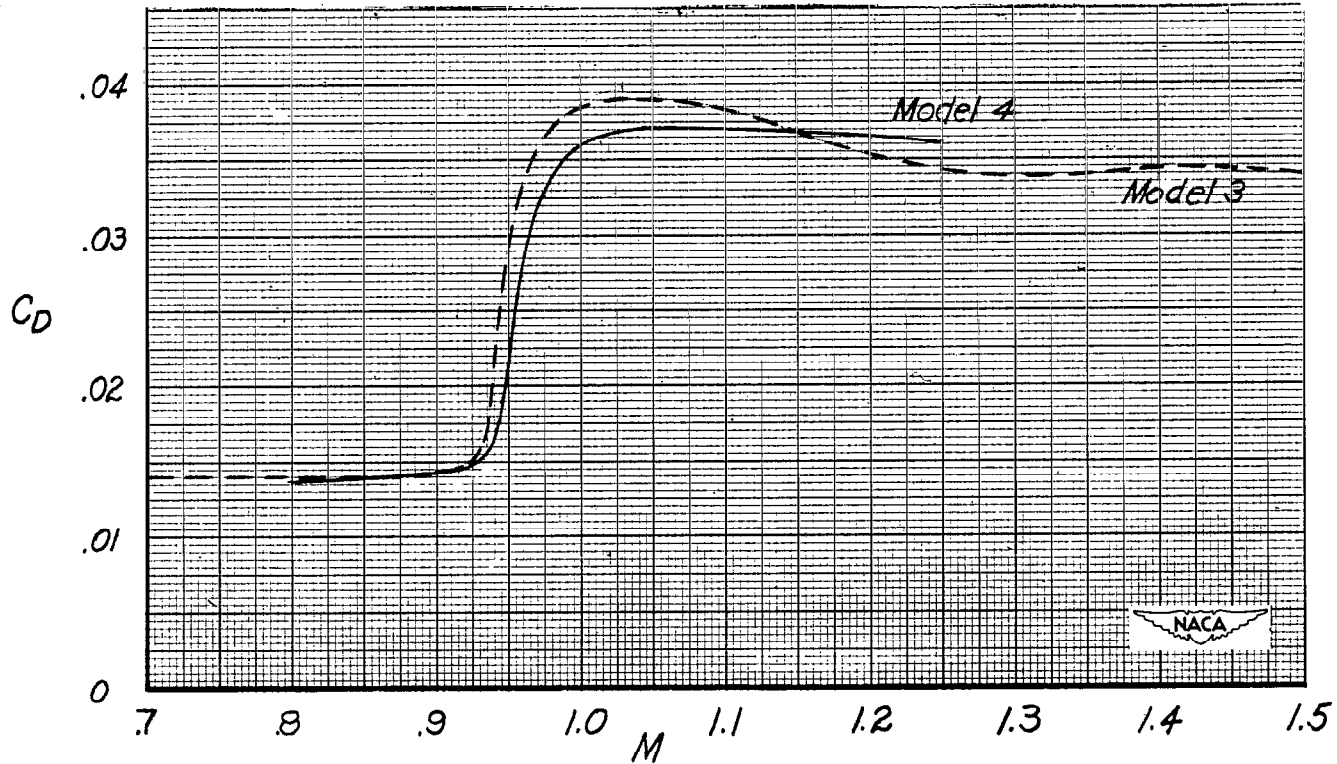


Figure 19.- Comparison of zero-lift drag coefficients of model 3 and model 4 with skin-friction drag coefficient corrected to wetted area at model 3.

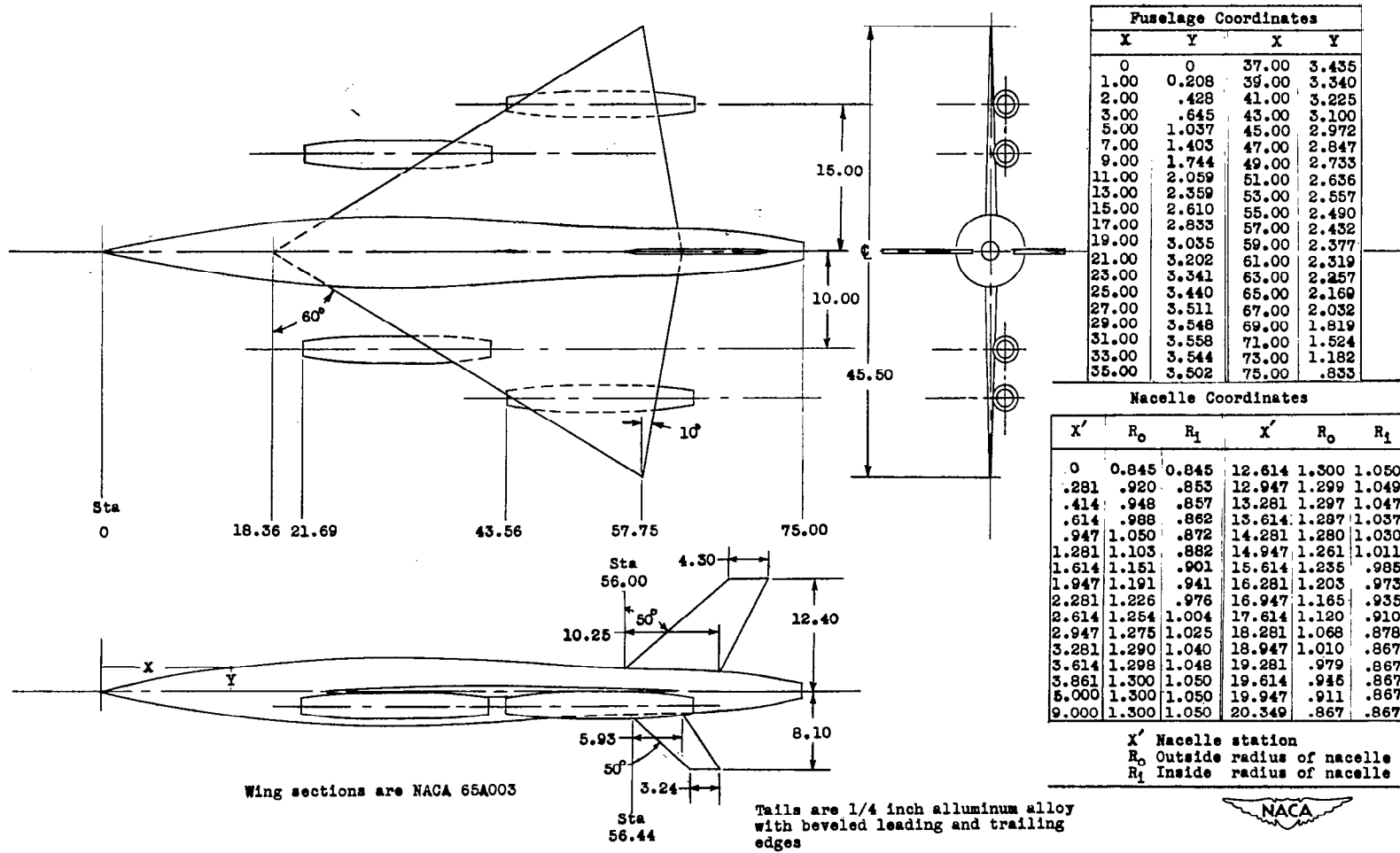


Figure 20.- Three-view drawing of model 5. All dimensions in inches.

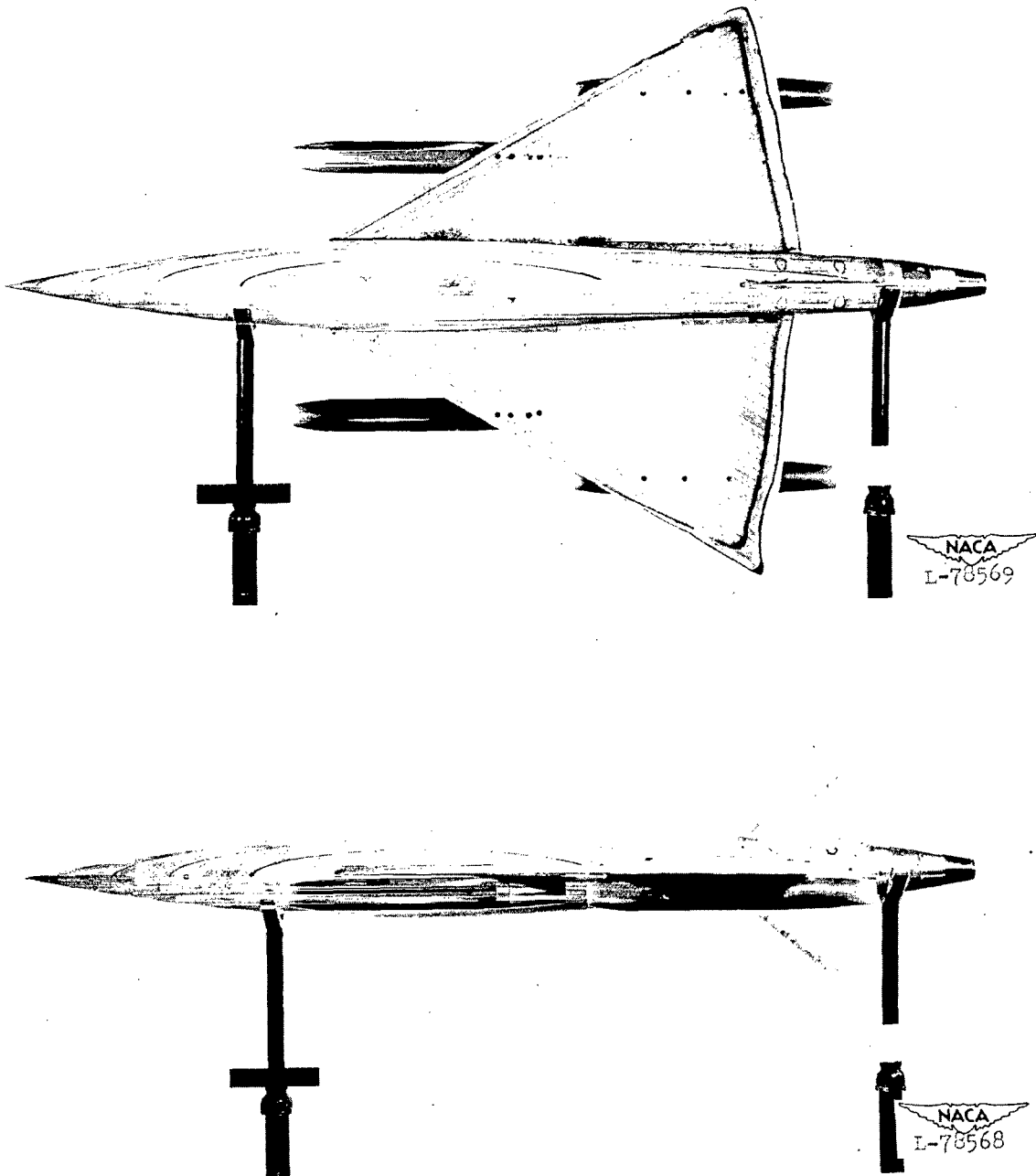


Figure 21.- Photographs of model 5.

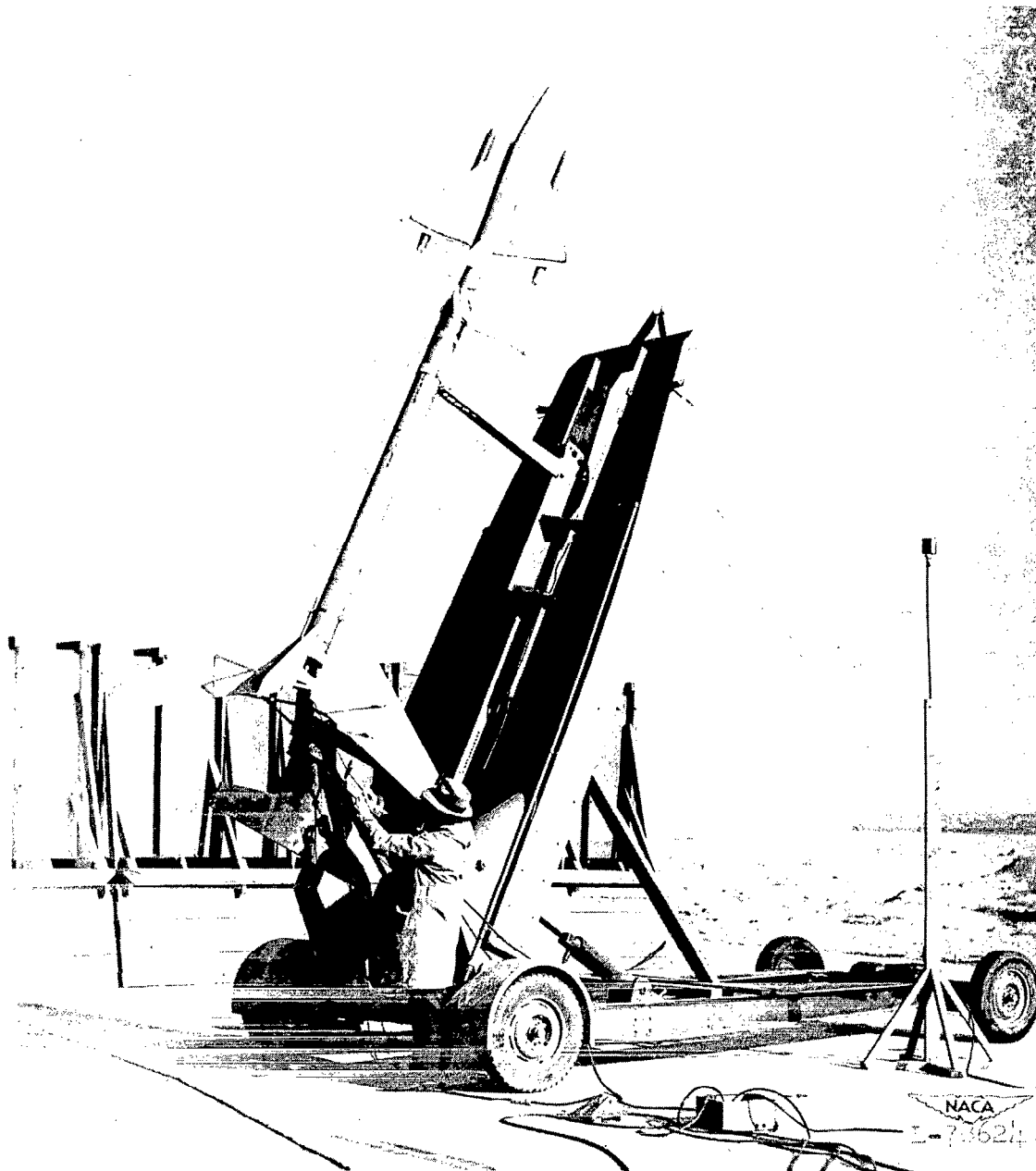


Figure 22.- Model 5 and booster on launcher.

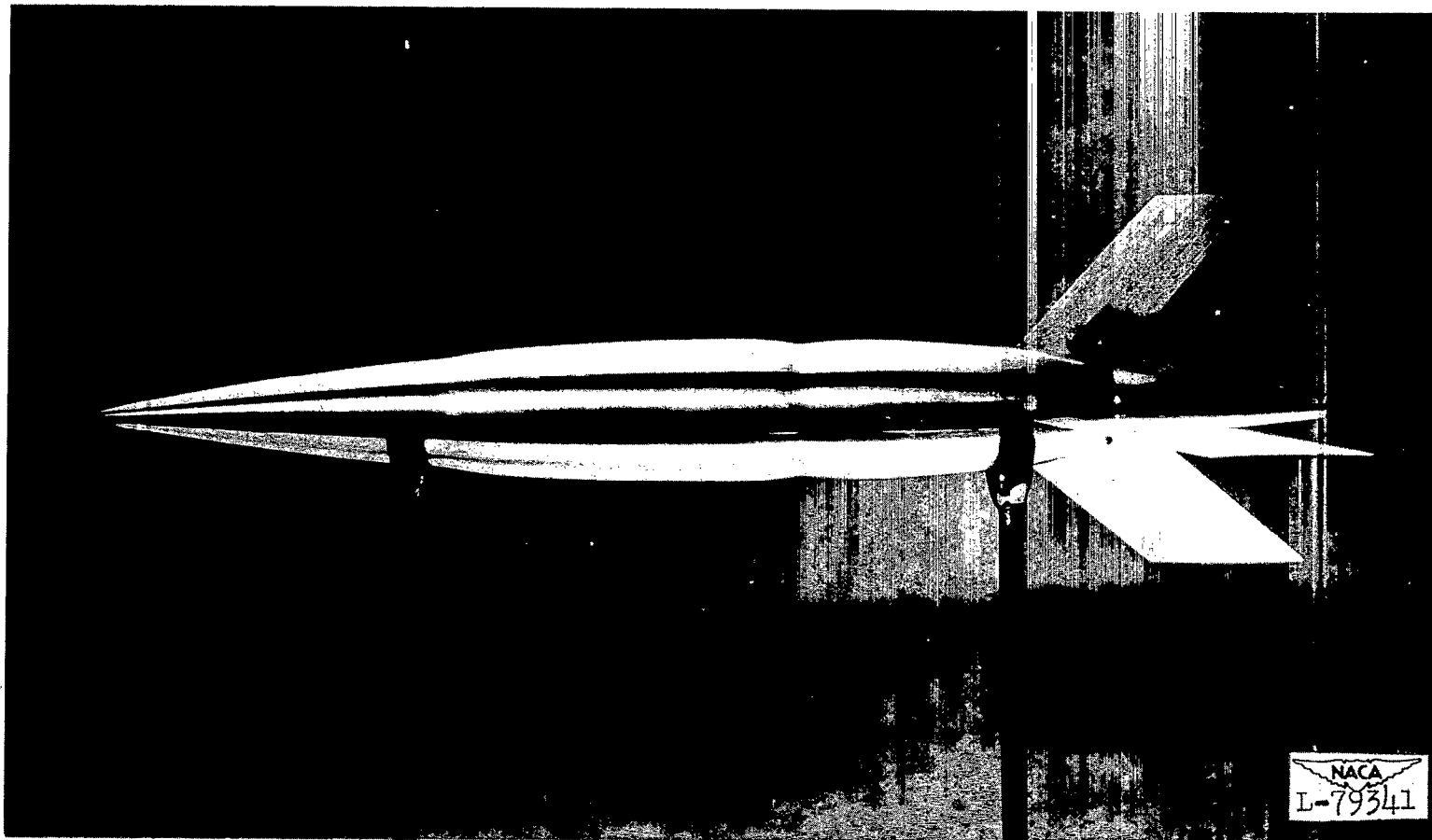


Figure 23.- Model 6. Model is a 1/82.5-scale body of revolution having the same longitudinal area distribution as model 5.

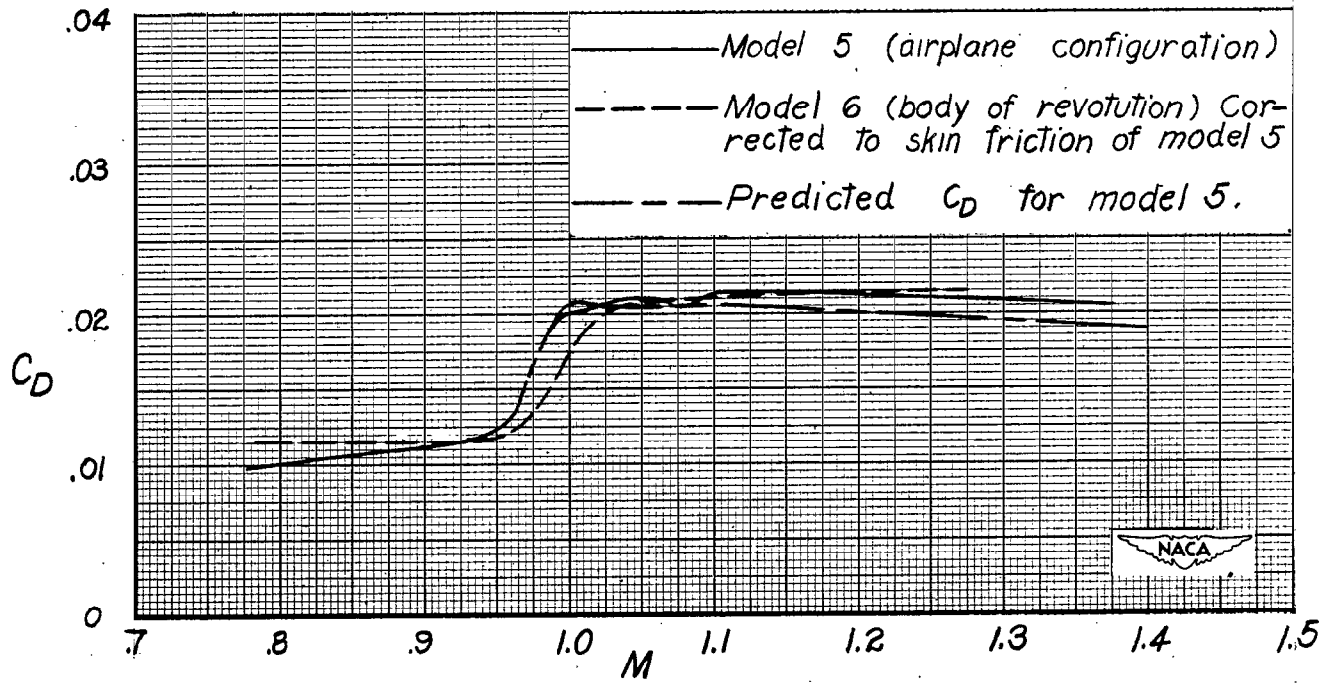


Figure 24.- Comparison of measured zero-lift drag coefficients of models 5 and 6 and the drag coefficient predicted for model 5 by the summation of isolated component drag coefficients.

SECURITY INFORMATION

NASA Technical Library

3 1176 01438 6008

